Mechanical Imaging of Soft Tissues with Miniature Climbing Robots

Artem Dementyev, Rianna M. Jitosho, and Joseph A. Paradiso.

***Abstract*— Systematically mapping the mechanical properties of skin and tissue is useful for biomechanics research and disease diagnostics. For example, later stage breast cancer and lymphoma manifest themselves as hard nodes under the skin. Currently, mechanical measurements are done manually, with a sense of touch or a handheld tool. Manual measurements do not provide quantitative information and vary depending on the skill of the practitioner. Research shows that tactile sensors could be more sensitive than a hand. We propose a method that uses our previously developed skin-crawling robots to noninvasively test the mechanical properties of soft tissue. Robots are more systematic and repeatable than humans. Using the data collected with a cutomoter or indenter integrated into the miniature robot, we trained a convolutional neural network to classify the size and depth of the lumps. The classification works with 98.8% accuracy for cutometer and 99.6% for indenter for lump size with a diameter of 0 to 10 mm embedded in depth of 1 to 5 mm in a simulated tissue. We conducted a limited evaluation on a forearm, where the robot imaged dry skin with a cutometer. We hope to improve the ability to test tissues noninvasively, and ultimately provide better sensitivity and systematic data collection.**

***Index Terms*— Lump detection, imaging, sensing, robotics, machine learning, skin**

I. Introduction

Systematically mapping mechanical properties of skin and tissue is useful in several applications, including disease diagnostics, cosmetics, and biomechanics. For example, some cancers are stiffer than normal tissues [1], [2] and typically are detected via palpation (touching by hand). This current method requires a doctor to perform the palpation, and consequently is disadvantageous because it does not provide systematic quantitative data. The latest advances in machine learning can improve measurement accuracy and resolution of complex tissues and aid doctors in noninvasive diagnostics. For example, machine learning techniques have shown promise in automatic detection of lung cancer [3] and kidney failure [4]. These machine learning techniques require systematic quantitative data. Since palpation is done by hand, there is a lack of quantitative data needed to apply machine learning techniques [5]. Also, prior research has shown that sensors could be more sensitive than human touch [6], [7], which suggests that a sensor designed for palpation may be better than a human at detecting nodes under the skin. Such a device would also generate the systematic quantitative data necessary to apply machine learning techniques for improving diagnostic accuracy. However, there are currently no accepted automated solutions to map the mechanical properties of the skin.

To address this issue, researchers have been developing sensor arrays that detect the mechanical properties of the skin. In the designs explored so far, a transducer makes repeated measurements over multiple points to generate a map. Existing research provides three methods of performing these measurements, and each method has associated challenges. The first method of measurement is manually applying a handheld tool to the skin. Some devices use an array of pressure sensors [8], [9]. Others measure deformation by capturing internal reflections of gel [10], or piezo oscillations [11], [12]. Cutometers [13]–[15] can also be used to measure deformation via suction or by using a rolling [16], [17] or dynamic [18], [19] or static [20] indenter. Independent of the sensing principle, handheld tools are operated manually, which introduces multiple issues. Because they are manual devices, there is the potential for inaccuracies and inconsistent applications of force. Moreover, handheld tools can only provide relative measurements. Lastly, human-operated devices may present privacy issues in situations without proper training. The second method of measurement is using a robotic arm to apply the transducer to the skin. For example, a tactile force sensor can be attached to the end-effector of a robot arm [21]. A challenge with this method is that the robot arm will create reaction forces, so the body limb has to be secured. Additionally, a large robot arm is expensive, and interfacing with it can be cumbersome. The third method of measurement uses non-contact measurements, such as Magnetic Resonance Imaging (MRI), to computationally estimate the mechanical properties of tissues [22]. These non-contact measurements can only provide relative estimates, and they can be inaccurate as tissues are complex. This type of measurement also requires large and expensive machines.

In this paper, we create and study a new measurement method to map mechanical properties. Our work differs from previous methods through the use of our previously developed Epidermal Robots platform (Fig 1), a small robot that can traverse the surface of the body. [23]. The robot uses suction to adhere to the skin, an array of sensors and motors to move, as well as onboard sensors to track its position. Utilizing Epidermal Robots for measurement of mechanical properties of skin provides several advantages:

1) No reaction forces. Applying forces locally prevents global reaction forces, which removes the need to secure the body joints during testing.
2) Easy deployment. Small robots can be shipped to people's houses or other remote locations.
3) Accurate localization for the mapping of measurements.
4) Repeatable measurements. Automated measurements ensure consistency and enable the use of machine learning techniques.
5) Less human labor. Measurements do not require highly trained person to do the examination.

In the remainder of this study, we first describe the Epidermal Robot and the measurement methods for mapping the skin properties. Specifically, we explore the use of two onboard sensors that could be integrated into the Epidermal Robot: an indenter as well as a cutometer. We then discuss our procedure for analyzing sensor data, which involves using convolutional neural nets (CNN) to detect the lumps' presence and size under the skin. We evaluate the performance of the custom CNN classifier from data collected by the sensors on simulated tissue. Finally, we do limited on-body testing to map dry skin on the forearm.

This paper was submitted for review on July 12, 2020. This work was supported by the MIT Media Lab Consortium.

A. Dementyev., was with MIT Media Lab, Cambridge, MA, US, He is now with the Google Research, CA, USA (e-mail: artemd@media.mit.edu).

R. M. Jitosho., was with MIT Media Lab, Cambridge, MA, US. Now she is with Stanford University (e-mail: rjitosho@stanford.edu).

J. A. Paradiso is with MIT Media Lab. (e-mail: joep@media.mit.edu).

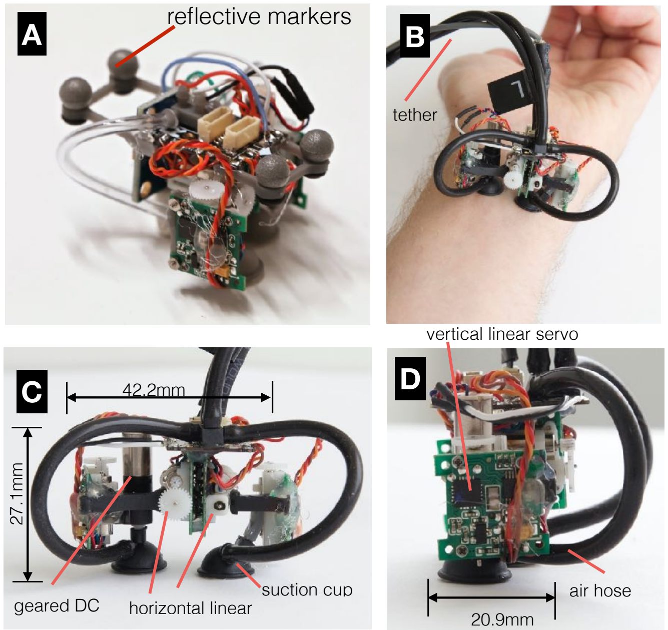

Fig. 1. Pictures of Epidermal Robots. A) Robot retrofitted with reflective markers for camera tracking. B) Robot on the arm. C) Front-view dimensions of the device. D) Side-view dimensions of the device.

II. Implementation

Design Overview

To quantify the mechanical properties of skin tissue, a force needs to be applied to the skin, and the response has to be measured. In this study, we adapted two commonly used sensors: a cutometer and an indenter. We chose these specific sensors as they can reasonably fit on a small robot.

Robot design

The sensors developed in this study are intended for use on Epidermal Robots. The design of these skin climbing robots has been described and evaluated in the previous work [23]. Epidermal Robots utilize 9 mm-diameter suction cups as a reliable and controllable way to adhere to the skin. For locomotion, the robot uses four linear servo actuators (SPMSA2005, Spektrum). The robot is tethered electrically and pneumatically to a control board with an ARM M4 microcontroller (Teensy 3.6, PJRC). The data is exchanged between the control board and PC over a serial port. A Java application was made to visualize and log the data on PC. The control board contains two miniature vacuum pumps (SC3101PM, Skookum Electronic co.) to generate a vacuum pressure of about -30 kPa for the suction cups. This board also measures the pressure for regulation purposes with two pressure sensors (MPXV611, NXP). The control board also coordinates the pressurization of the suction cups and the motion of the linear servo actuators for locomotion controls. Aside from the electronic sensors and actuators, the robot's parts are 3D printed with an SLA printer (Form 2, Formlabs, Black resin V4). During movement, the robot requires about 1.21 Watts, provided from the tether. The weight of the robot is 10 grams. The robot can crawl at a maximum speed of 31 cm/min, but runs slower during indenter and cutometer measurements. The robot can climb on curved body surfaces of radii above 4.4 cm, which includes an adult-sized torso (12 cm), but not a wrist (2.5 cm). The robot can move on vertical surfaces and upside down, assuming the tether is properly supported.

Cutometer: measuring with suction

A cutometer applies suction to the skin and measures how the skin deforms under negative pressure. In our work, we apply the same principle as illustrated in Figure 2. Since the feet of the robot already have suction cups, they can be readily augmented with a small off-the-shelf infrared proximity sensor (GP2S60A, Sharp). In our design, we mounted the sensor on a custom-designed printed circuit board (PCB) and glued it with epoxy inside a specially designed suction cup. To comply with the infrared light-emitting diode (IR LED) current limit, the current was limited to 21 mA with a 100 Ohm resistor.

The infrared proximity sensor simultaneously emits 950 nm wavelength light out of its IR LED while detecting the reflected light with a phototransistor. At this wavelength, the skin reflects some of the infrared light. As the distance between the sensor and the skin increases, there is more scattering, and the phototransistor detects less light. This sensor allows for the measurement of skin properties because we expect the skin to displace less in a vacuum if there is a lump underneath the skin surface. This is illustrated in Figure 2A. To characterize a given tissue sample and to alleviate external influences on the reflectance, we fit the raw infrared data during suction (e.g., Figure 2C) to an exponential function:

$$f(x) = ae^{-bt} + c \tag{1}$$

Where *a,b,c* are constants specific to the curve and t is time (sec). A heat map can be generated based on the parameter values measured at discrete points over the surface of a tissue sample. Example heat maps are shown in Figure 3. We found that the parameter *a* provides the most relevant information for detecting and characterizing lumps underneath the skin surface. We visually compared heat maps produced with parameter *a, b,* and *c* and found parameter *a* to better reflect the simulated lump. This parameter is the scaling factor in the exponential function fitted to the IR data and is affected by the sensor's relative location to the lump.

Indenter: measuring force and deformation

An indenter-based technique is another common way to measure the elasticity of the skin [18]–[20], [24]. Also, such a technique is used in durometers for quick non-destructive hardness testing of a material such as rubber or metal. This is done by creating an indentation on the material with a known force, and then measuring the resulting depth of indentation. Hardness is correlated with tensile strength and elastic modulus, so in this work, we use a similar approach to measure the elastic modulus of skin.

Elastic modulus is the slope of the stress-strain curve in the elastic linear region during unilateral loading. It is a useful parameter as it provides an absolute way to quantify a material. An equation for the elastic modulus is:

$$E = \frac{stress}{strain} = \frac{F/A}{\Delta L/L_0} \tag{2}$$

Where F is the force (N), A is the area and ΔL is the change in length and L_0 is the original legnth.

Measurement methods with an indenter provide an approximation to the elastic modulus of the soft tissue compared to tensile testing [25]. However, while tensile testing is more accurate, it is not possible to apply this method noninvasively. It requires a prepared bulk sample and a universal testing machine with unilateral loading. For this reason, we chose an indenter method. Additionally, while dynamic measurements provide insight from cycling testing, we restrict our methods to static measurements due to practical limitations such as the speed and robustness of our linear servos.

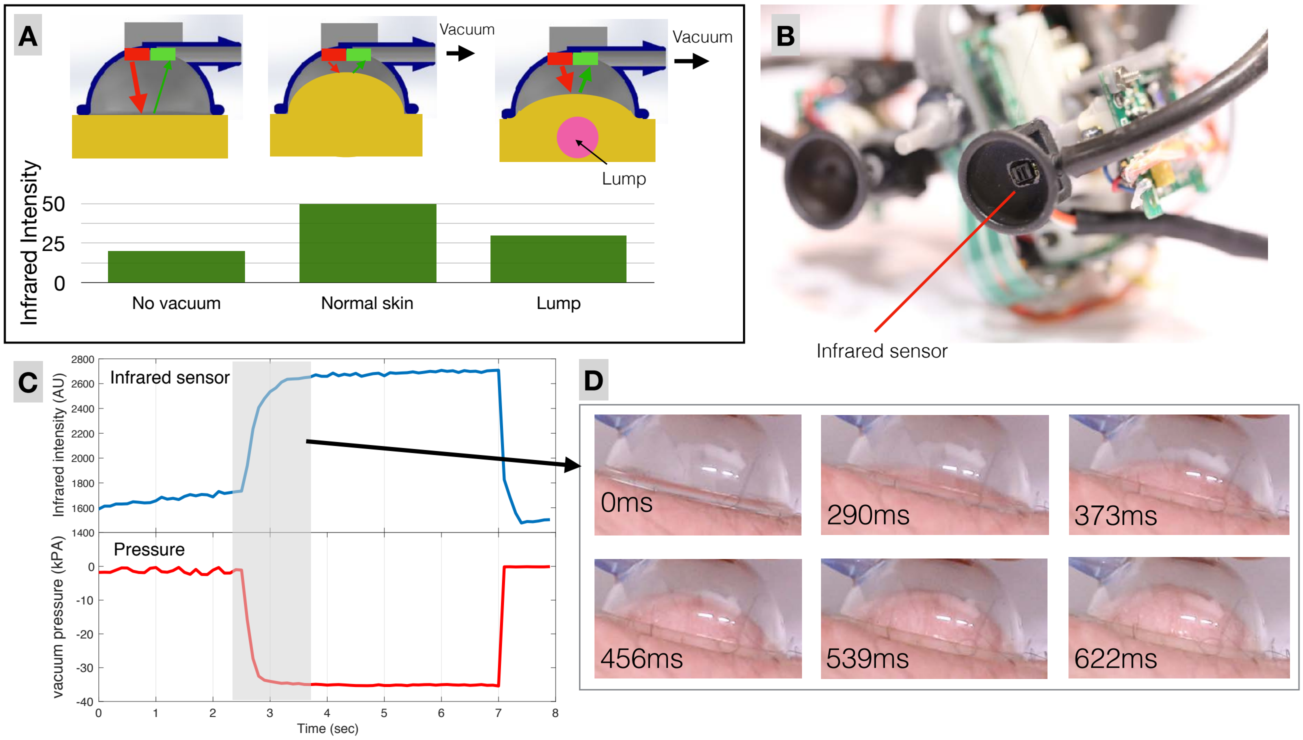

Fig. 2. Cutometery sensing principles with the robot. A) A graphical representation of the cross-section of the suction cup and the skin. The red arrow represents transmitted infrared light, and green is the light reflected back to the sensor. The skin with the lump bulges less under vacuum than the skin without the lump. B) The Epidermal robot with an infrared sensor integrated into the suction cup. C) Raw data from an infrared sensor and pressure before and after suction is applied to the skin. The suction cup moves closer and closer to the skin before attachment, so infrared intensity increases during baseline. D) The images of skin bulging under suction with a clear suction cup.

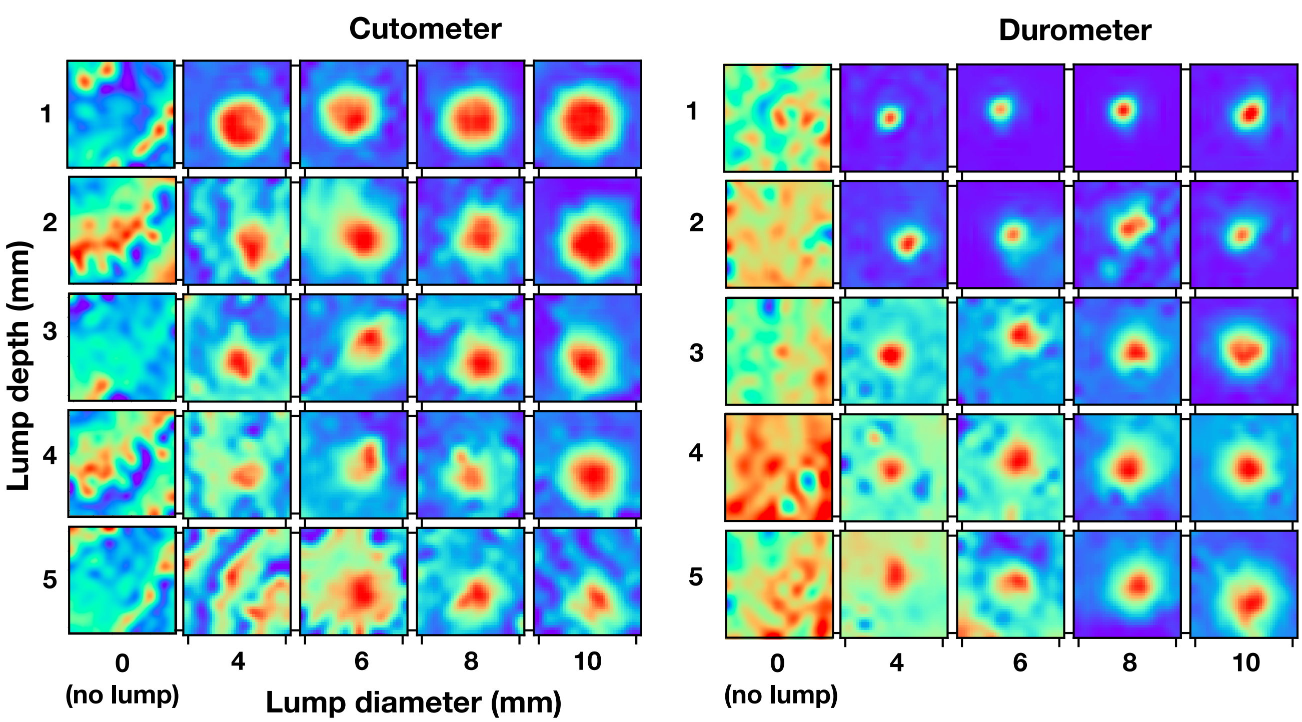

Fig. 3. Example of 11x11 pixel heat maps collected by cutometer and indenter for different lump depth and diameter in the simulated tissue. There are 11x11 pixels with an individual size of 2x2 mm. To improve visual clarity, each heat map is colored in relation to itself only. Bessel interpolation was applied to all samples.

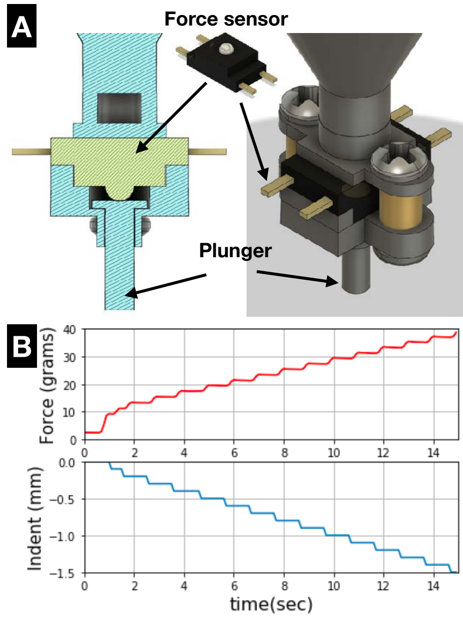

Fig. 4. Indenter sensing principle. A) The design of the force sensor indenter. On the left is a cross-section view of the plunger assembly. The force sensor is sandwiched between two 3D printed pieces. The plunger has a clearance to move freely. On the right is the isometric view of the assembly. B) The data collected by the indenter includes simultaneous measurement of force and indent over time.

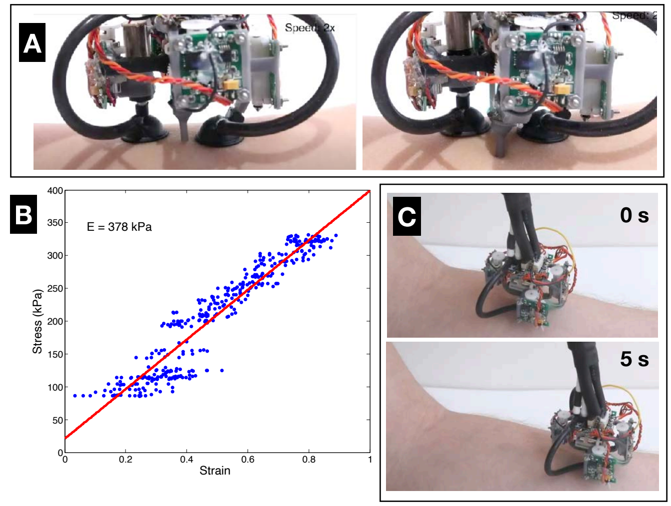

Fig. 5. Robot equipped with an indenter. A) The robot makes an indentation on the skin. B) Example strain vs stress graph obtained from one measurement on the skin. C) The robot walking on the forearm, as it makes indenter measurements.

In our design, we modify the durometer to allow us to measure the applied force (stress) and deformation (strain) simultaneously. Force is measured using a miniature force sensor (FSS1500NSR, Honeywell). The signal is conditioned with a Wheatstone bridge, amplified and passed through a high resolution (24-bit) analog-to-digital converter (HX711, AVIA semiconductor). The force sensor was fitted with a custom-designed 3D-printed tip with a diameter of 3 mm, allowing for easy calculation of stress. The indenter design is shown in Figure 4.

To calculate the elastic modulus of the skin, we apply a known deformation and measure the resulting force on the indenter. We can plug these data values directly into the elastic modulus equation. Specifically, we calculate the stress applied to the indenter at discrete displacements ranging from 0 to 1.5 mm indentation with 0.1 mm intervals. From this data, we obtain the slope from a linear fit, which is the elastic modulus. We assume that L_0 is 1.5 mm. The displacement of the indenter was limited by the size of the robot and the displacement of the linear servo motors.

The simulated tissue testing was done using a force sensor. However, we found that the force sensor is too large to fit into the current robot. To fit the robot with an indenter, we replaced the force sensor with a force-sensing resistor (FSR) as a proof-of-concept. Specifically, we used FSR400 (Interlink Electronics). While FSRs are smaller and allow for decreasing sensor size, the measurements were nonlinear and noisy, requiring more complicated data processing. We used two linear motors (SPMSA2005, Spektrum) to push the indenter into the skin. We used two motors to increase the pushing force and position the rod between the two suction cups. If the rod were offset from the middle, the robot would tilt during the pushing, potentially causing detachment from the skin. The displacement of the rod was extracted by digitizing the voltage from the potentiometer of the servo that is used as an encoder. Figure 5, shows the robot equipped with the indenter.

The robot has to be well and stably attached to the skin, as the force exerted by the rod into the skin is transferred to the suction cups. To prevent detachment as well as influence the measurements, this force has to be less than the attachment force of the robot.

Simulated tissue fabrication

To characterize our cutometer and durometer sensors, as well as to provide ground truth for training a supervised neural network to classify sensor data, we draw from previous works on generating simulated tissue [6], [8], [9]. In this work, tissue samples were created by utilizing silicone (Ecoflex 00-30, Smooth-On) mixed with 2% (by weight) flesh color pigment (Silc pig, Smooth-On). Ecoflex 00-30 is frequently used to mimic biological tissues. Skin has an elastic modulus between 2.8 - 31.9 kPa, while Ecoflex 00-30 reported values are 22.1 - 125 kPa [26], [27]. The silicone samples are comparable to the skin in mechanical properties and color, which is important for collecting realistic data with the cutometer's infrared sensor.

For fabrication, an acrylic cube was used as a mold. To simulate lumps under the skin, hard 3D printed plastic balls (Black resin V4, Form 2, Formlabs) with an elastic modulus of 2.8 GPa [28] were embedded in the silicone. The lumps were suspended at different heights in silicone by fixing them on a small and stiff optical fiber, which was removed after the silicone was cured. Figure 6B shows a suspended 3D printed ball prior to filling the mold with silicone. Lumps were stiffer than biological lumps [1] but provide an appropriate comparison with previous literature that employes other plastic ball materials such as Delrin [6] with approximately 3.1 GPa elastic modulus [29]. The elastic modulus of ductal carcinoma has been shown to be 460-580 kPa [1]. This provides around 1:18 to 1:29 contrast from the fat tissues. Using an elastic modulus of 125 kPa for Ecoflex 00-30, the contrast is around 1:22 with the 3D printed lumps.

Lumps of various sizes (4,6,8,10 mm diameter) were embedded at different heights (1,2,3,4,5 mm), as demonstrated in Figure 6. A sample without a lump was also fabricated, resulting in a total of 21 simulated tissue samples.

Training Data Collection

Since neural networks require a lot of training data, generating sufficient sensor data with each of the simulated tissue samples is

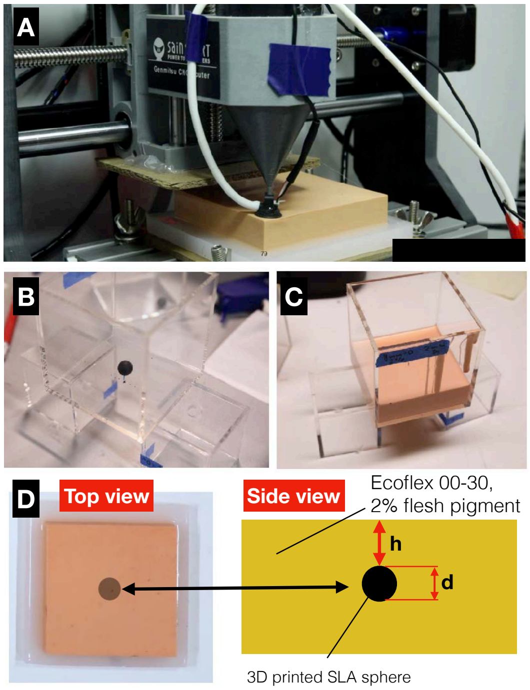

Fig. 6. Testing of simulated tissue. A) CNC machine loaded with the silicone tissue sample and cutometer head. B) The mold for test tissue, before pouring the silicone. C) The mold after the silicone is poured. D) Left, the top view of the silicone tissue, showing the location of the simulated lump. Right, the side view cross-section of silicone tissue, showing the height and diameter parameters.

a time-intensive task. For example, data collection for this study required a total of 125 hours. Since the current robot prototype is not robust enough for such a task, we modified the head of a CNC machine to move the suction cup or indenter to simulate the walking of the robot.

An off-the-shelf, inexpensive 3-axis Computer Numerical Control (CNC) router (Genmitsu, 1810-PRO) with a resolution of 0.1 mm was modified for testing, as shown in Figure 6. The CNC machine allows motorized control of 3-axis from software, and is commonly used for machining. The CNC spindle was replaced with a 3D printed adapter head (PLA material on Prusa Mark 2) for attaching the suction cup or the indenter. The CNC router was controlled with an ARM M4-based microcontroller (Teensy 3.6, PJRC) by sending G-code (machine control code) commands over serial to the motor control board. The microcontroller also sampled the pressure sensors and infrared sensors at 14-bit resolution and sent the data to the PC for visualization and data storage in real-time with a Java application.

The head moved with a step size of 2 mm, which provided the minimum sampling resolution for the smallest lump (4 mm). For each test run, an 11 by 11 array of data points was collected, for a total of 121 points. The data were combined into an 11x11 grayscale image for further processing. Each simulated tissue sample was tested 15 times, thus providing 315 distinct images.

Classifier Architecture

The collected images were used to train a supervised neural network with 21 output classes (no ball, and combinations of four diameters and five depths). TensorFlow and Keras libraries [30] were used to implement the machine learning techniques. Convolutional neural nets (CNNs) have previously been shown to be a capable architecture for image data. Thus, we used CNNs with Relu activation. It was followed by a fully-connected layer with 50 neurons

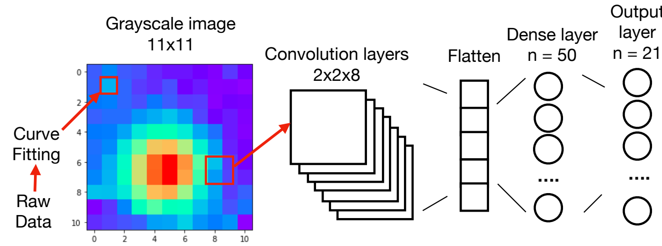

Fig. 7. The flow diagram of the convolutional neural net used to classify the diameter and depth of the simulated lump tissue.

and Sigmoid activation. Finally, a dense output layer with Sigmoid activation. Classifier model, as shown in Figure 7. For training, we used 80-20% train and test split with a shuffle. The indenter model was trained over 200 epochs with a batch size of 100. The cutometer model had 400 epochs and a batch size of 100. We used the Adam optimizer with a 0.01 learning rate.

To avoid using training data in validation, 20% of the data was not used in training the model. It was used to determine accuracy in the evaluation section. The data was split randomly in each training/validation.

We decided to use a machine learning approach versus a simpler fitting approach (e.g., fitting a function on a heat-map) for the following reasons. First, machine learning has shown to be a promising technique in medical imaging [31], as well as it is an industry-standard in image recognition and classification, such as of human faces [32]. Second, there is a large variety of skin (dryness, color, age variations) that a conventional signal processing approach would have difficulty in capturing. With a large amount of diverse data, it is potentially possible to train a well-generalized model. Third, the machine learning approach could be easily adapted to various sensing methods, as we show here that the same network architecture works for two sensing approaches. Also, the network could be adapted to the fusion of multiple sensors.

Localization on human body

To utilize cutometer and indenter sensors on Epidermal Robots, the robots must know where they are collecting the data on the human body. This requires localization as well as a global map of the body. In our previous work [23], [33], we proposed a localization technique based on motion capture. We retrofit the robots with 4 infrared 3 mm reflective balls. Motion capture cameras (Prime 13, Optitrack) track the ball positions to determine robot location and orientation. The 3D shape of the body is captured with an off-the-shelf 3D scanner (Sense2, 3D Systems). Finally, reflective balls are placed on the body to compute the orientation of the body in relation to the robot.

Alternatively, tracking could be done using an inertial tracking and odometry system. However, as explored in our previous work, the drift in this approach is too large for this application. It is advisable to reduce the error in the future so that external tracking is not required.

III. Evaluation

Simulated lump model results

The mean accuracy of ten models is reported here. Due to a small data set, each time, the model was retrained and evaluated with a random shuffle. A confusion matrix of the agreggated cutometer results is shown in Fig 8. The indenter had only a few misclassifications. The classification accuracy between no lump vs. samples with lumps was at 100% for cutometer and indenter. However, some errors occurred

True Label (size/depth in mm) / Predicted Label (size/depth in mm)

	none	4/1	4/2	4/3	4/4	4/5	6/1	6/2	6/3	6/4	6/5	8/1	8/2	8/3	8/4	8/5	10/1	10/2	10/3	10/4	10/5
none	123	0	0	0	0	0	0	0	0	0	0	0	0	0	0	0	0	0	0	0	0
4/1	0	25	1	0	0	0	0	0	0	0	0	0	0	0	0	0	0	0	0	0	0
4/2	0	3	23	0	0	0	1	0	0	0	0	0	0	0	0	0	0	0	0	0	0
4/3	0	0	0	28	0	0	0	0	1	0	0	1	0	0	0	0	0	0	0	0	0
4/4	0	0	0	0	31	0	0	0	0	0	0	0	0	0	0	0	0	0	0	0	0
4/5	0	0	0	0	0	29	0	0	0	0	0	0	0	0	0	0	0	0	0	0	0
6/1	0	3	2	0	0	0	25	0	0	0	0	0	0	0	0	0	0	0	0	0	0
6/2	0	0	0	0	0	0	0	28	0	0	0	0	0	0	0	0	0	0	0	0	0
6/3	0	0	0	0	0	0	0	0	26	0	0	0	0	0	0	0	0	0	0	0	0
6/4	0	0	0	0	0	0	0	0	0	37	0	0	0	0	0	0	0	0	0	0	0
6/5	0	0	0	0	0	0	0	0	0	0	25	0	0	0	0	0	0	0	0	0	0
8/1	0	0	0	2	0	0	0	0	0	0	0	23	2	0	0	0	0	0	0	0	0
8/2	0	0	0	1	0	0	0	0	0	0	0	1	17	0	0	0	0	0	0	0	0
8/3	0	0	0	0	0	0	0	0	0	0	0	0	0	31	0	0	0	0	0	0	0
8/4	0	0	0	0	0	0	0	0	0	0	0	0	0	0	32	0	0	0	0	0	0
8/5	0	0	0	0	0	0	0	0	0	0	0	0	0	0	0	26	0	0	0	0	0
10/1	0	0	0	0	0	0	0	0	0	0	0	0	0	0	0	0	27	0	0	0	0
10/2	0	0	0	0	0	0	0	0	0	0	0	0	0	0	0	0	0	25	0	0	0
10/3	0	0	0	0	0	0	0	0	0	0	0	0	0	0	0	0	0	0	24	0	0
10/4	0	0	0	0	0	0	0	0	0	0	0	0	0	0	0	0	0	0	0	34	0
10/5	0	0	0	0	0	0	0	0	0	1	0	0	0	0	2	0	0	0	0	0	26

Fig. 8. Confusion matrix for cutometer for identifying lumps of different diameters and depths. Each matrix shows aggregated labels from 10 models. Due to random shuffle, the number of samples in each class slightly varies.

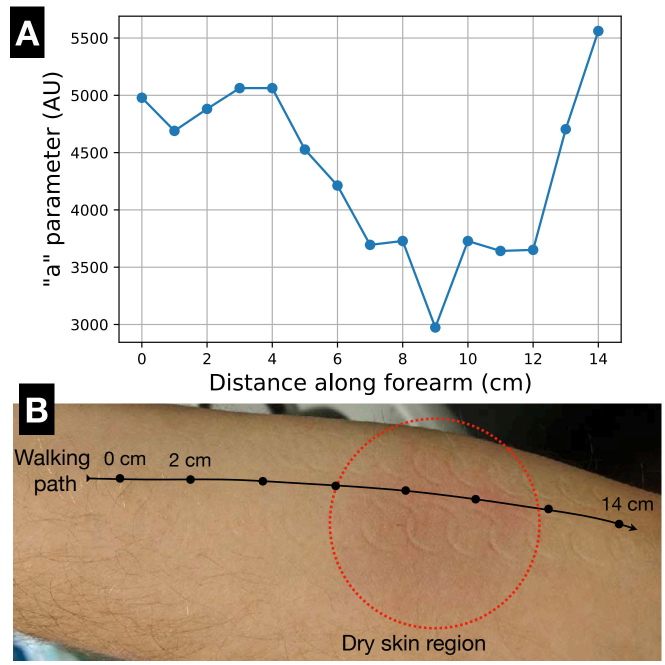

Fig. 9. IR sensor data, captured by robot moving on the arm over a dry spot. A) Measurements from each step as the robot moved forward. B) Picture of the forearm with overlaid robot path and circled dry skin region.

between the classification of different lump diameters and depths. Below is a more detailed discussion of the errors.

For cutometry, we obtained 98.8% (std:±0.3%) validation accuracy. The misclassification mostly occurred with the 4 mm lump misclassified as a 6 mm lump and vice-versa. Also, there were misclassifications between 1 and 2 mm depths for the 4 mm lump. Looking into the raw data, as visualized in Figure 3, the misclassified cases look similar. The instrument does not seem sensitive enough in those cases. Increasing suction pressure might improve sensitivity.

Using an indenter, a higher validation accuracy of 99.6% (std:±1.1%) was obtained. In some cases, 4 mm lump at 4 mm depth was classified as at 3 mm depth.

Cutometer forearm validation

We conducted a limited experimental validation on healthy skin. We fitted both of the robot's suction cups with IR sensors that we described earlier. We used a hot air gun with a temperature set at 100 Celcius and dried a patch of the skin for 5 minutes. The hot air gun was held about 10 cm away from the skin to avoid causing pain. Dehydrating the skin decreases the modulus of elasticity [34]. We expected a change in the *'a'* parameter, as shown in Equation 1. After the skin was dried , the robot walked 30 steps on the forearm and collected data for each 15.4 mm step from the two IR sensor inside the suctions cups. To avoid gravity effects from the tether, the forearm was placed horizontally.

The robot took approximately 3 minutes to complete the task. Results from one suction cup is shown in Figure 9. There is a large decrease in the *'a'* parameter as the robot walked on the dried skin, vs. normal skin.

Measuring elastic modulus with indenter robot

For the robot with the indenter, we collected data from a single point on the forearm. We were interested to see if we could measure the modulus of elasticity from the indenter. We placed the robot on the forearm for the measurement.

The results are shown in Figure 5B. To extract the elastic modulus, we use a linear fit. Comparing the raw data in Figure 5B to Figure 4B shows that the FSR-based sensing is noisier than the force sensor.

The skin elastic modulus has large variations, as reported in the literature. It greatly depends on whether it is in-vivo or in-vitro testing, the type of testing machine, and the location of the test [35]. In our case, we compare to Young modulus for indentation testing on the limbs and in-vivo only. Our elastic modulus is somewhat higher (378 kPa) than what is reported in the literature for indentation. One study reported 10.4 to 89.2 kPa [36] for lower limbs, while another study reported 21 to 195 kPa [37]. One of the main sources of noise and error is the FSR.

Discussion

Comparison between cutometer and indenter

The cutometer and indenter have different advantages and disadvantages. The cutometer does not require any moving parts and is easily integrated into the robot, as suction is already used for adhesion. As a disadvantage, it does not provide absolute measurements, as the infrared light is affected by the skin properties and state. For example, skin discolorations can affect the reflectance, however more sophisticated sensing such as time-of-flight infrared can mitigate that. Furthermore, the resolution is limited by the size of the suction cup, which is 9 mm in diameter currently. The indenter has a higher resolution as the diameter of the tip is only 1 mm. Also, an indenter can provide absolute measurements, as it is not affected by skin surface properties. As a disadvantage, the indenter requires two additional motors, which reduced the robustness of the sensing method. Also, the indenter is significantly slower: each measurement can take up to 15 seconds vs. 5 seconds with a cutometer. During measurements, the speed is 6.2 cm/min for the indenter and 18.5 cm/min for the cutometer, with a 15.4 mm step size. Without sensing, the speed is 31.0 cm/min. Potentially, the measurements from the indenter and cutometer could be fused. The cutometer could be used to quickly identify areas that need attention. The indenter could go over those areas with higher resolutions and accuracy but slower speed.

Comparison to previous work

Although it is challenging to compare the experiments directly as the different studies had unique setups, we will attempt to make comparisons in general terms. Closest in testing is the work by Li et al. [9], which used a 9x9 element soft indenter array. This work did not use a machine learning approach for lump classification. The experiment on simulated tissue reported an error of 2% and a standard deviation of 12% for lump size classification. In contrast, using an indenter, we obtained a slightly better error of 0.4% and a lower standard deviation of 1.1%).

Simulated tissue vs. real tissue

There are some differences between the simulated tissue setup and real skin. While we were able to obtain valid measurements from both, we want to highlight the differences here.

The simulated tissue was laid flat, so gravity did not play a role. We tested the forearm on a flat surface as well. The human body might cause the robot to be at a different angle due to curvature. While the robot can traverse torse, arms, and legs, this might affect the measurements. Futhermore, the localization on the human body is more complex. External camera tracking can be accurate but difficult to set up at a remote location. Alternatively, a "dead-reckoning" approach could be used with onboard sensors, using IMUs and encoders. The localization is also needed to avoid and track missing steps. On real tissue, the robot might miss a step due to inability to attach.

In the simulated tissue, the indenter is pushing against the router while fixed in a rigid frame. In the forearm experiment, the robot pushes against it's attached legs. Since the skin is elastic, this can cause stretching of the skin under the suction cups, affecting the measurements. This could be more profound at higher indentations, as higher force is applied to the skin. We tried to control for this effect by making a minimal indentation of 1.5 mm. We have not seen this effect in Figure 5, and the force appears to be linearly proportional to displacement.

Applications

In this paper, we focus on a diagnostic use case by using Epidermal Robots to image skin mechanical properties and lumps. Beyond medicine, we believe there are other applications of these techniques. The applications are especially appealing where a large machine cannot be used, such as at home or in a remote location.

For example, this approach can potentially be used for more comfortable and effective sockets for limb prosthetics. Ideally, a limb prosthetic should have variable stiffness to match the mechanical properties of the limb, but this requires a map of the limb's mechanical characteristics. If such a map is obtained, a multi-material printer can print a custom socket with variable stiffness. Currently, the socket fitting process is done manually. Researchers have been exploring multi-indenters [38] or camera-based imaging [39]–[41] for such measurements. Such approaches require specialized and large machines. The Epidermal Robots can be used to map the stiffness at home without the need for large machines. Beyond prosthetics, mechanical mapping properties can be used to make more comfortable clothing for sports applications.

Another area is cosmetics and personal care. Currently, the effectiveness of new skincare products (e.g., cremes) is measured using a cutometer. Such an approach provides limited data and could be enhanced by systematically taking multiple measurements over an area. However, the robot should be miniaturized for face use.

Furthermore, applications could include biomedical research studies and spatial imaging of skin and tissue disorders. Also, this mapping technique could be used on large animals as well.

Limitations and Future Work

As the focus of this paper is technology development, the work was conducted on a simulated tissue. Only a limited proof-of-concept study was done on a human forearm. Real lumps were not tested. To fully understand this approach's usability, an extensive study with multiple patients and skin locations would have to be conducted. Ideally, the study would image the lumps using the robots compared to a gold-standard such as manual palpation MRI, CT, or ultrasound.

For the scope of this work, we focused on two sensing methods and a limited depth of only 5 mm. In the future, we hope to explore other ways to allow 3D imaging inside the body. We hope one day, the robot could provide data similar to CT/MRI scanners. For example, a robot equipped with infrared light and a time-of-flight detector could be used for diffuse optical tomography. This technique allows 3D imaging inside the body. Robots could even potentially be equipped with an ultrasound probe for the same purpose. With advanced imaging techniques, the sensitivity could potentially be increased to detect early signs of cancer such as microcalcifications in breasts.

Furthermore, we plan to improve the machine learning approach to extrapolate information beyond lump presence and size. For example, if the robot could flag, detect medical issues, and improve diagnostics accuracy.

There are technical limitations to the robots that affect the usability of robots in the real-world. However, we believe those limitations can be overcome with more development. One limitation is a tether, which could be dispensed with by further component miniaturization. The current scan time is slow, with each indenter measurement taking 15 sec. To decrease the scanning time, we hope to explore how multiple robots could work together. Lastly, localization requires an external camera setup, but a localization technique that is fully integrated into the robot is preferred; we have explored an initial attempt at this in previous work [23], [33].

The effects of gravity on the measurements will need to be studied and accounted for in the untethered version. In the current version, it is hard to uncouple the influence of the tether from gravity.

IV. Conclusion

In this paper, we demonstrate the potential for small robots to systematically map the human body. This technique can provide advantages over handheld tools such as easy deployment, privacy, repeatable measurements, and localization. To validate this idea, we first conducted sensor-level testing by fitting a CNC router with custom indenter and cutometer sensors and characterized sensor performance on simulated lump tissues. Using supervised neural networks, the classification accuracy of lump size and depth was 99.6% for the indenter and 98.8% for the cutometer. After these initial promising results, we integrated the sensors on the Epidermal Robots platform. The cutometer sensors were embedded into the suction cups with no changes. The indenter sensor was switched to an FSR due to size constraints. In the final validation experiment, the cutometer robot walked on a forearm with a patch of dry skin. The data shows that dry skin was successfully distinguished. The indenter robot was tested on a single spot due to technical limitations, but it was able to determine the local skin elasticity. We believe that our approach provides a new way to measure the human body for various applications, including medicine, cosmetics, biomechanics, and clothing.

References

[1] T. A. Krouskop, T. M. Wheeler, F. Kallel, B. S. Garra, and T. Hall, "Elastic moduli of breast and prostate tissues under compression," *Ultrasonic imaging*, vol. 20, no. 4, pp. 260–274, 1998.

[2] A. Lyshchik, T. Higashi, R. Asato, S. Tanaka, J. Ito, J. J. Mai, C. Pellot-Barakat, M. F. Insana, A. B. Brill, T. Saga *et al.*, "Thyroid gland tumor diagnosis at us elastography," *Radiology*, vol. 237, no. 1, pp. 202–211, 2005.

[3] D. Ardila, A. P. Kiraly, S. Bharadwaj, B. Choi, J. J. Reicher, L. Peng, D. Tse, M. Etemadi, W. Ye, G. Corrado *et al.*, "End-to-end lung cancer screening with three-dimensional deep learning on low-dose chest computed tomography," *Nature medicine*, vol. 25, no. 6, p. 954, 2019.

[4] M. Makino, R. Yoshimoto, M. Ono, T. Itoko, T. Katsuki, A. Koseki, M. Kudo, K. Haida, J. Kuroda, R. Yanagiya *et al.*, "Artificial intelligence predicts the progression of diabetic kidney disease using big data machine learning," *Scientific reports*, vol. 9, no. 1, pp. 1–9, 2019.

[5] T. Panch, H. Mattie, and L. A. Celi, "The "inconvenient truth" about ai in healthcare," *NPJ Digital Medicine*, vol. 2, 2019.

[6] J. C. Gwilliam, Z. Pezzementi, E. Jantho, A. M. Okamura, and S. Hsiao, "Human vs. robotic tactile sensing: Detecting lumps in soft tissue," in *2010 IEEE Haptics Symposium*, March 2010, pp. 21–28.

[7] A. L. Trejos, J. Jayender, M. Perri, M. D. Naish, R. V. Patel, and R. Malthaner, "Robot-assisted tactile sensing for minimally invasive tumor localization," *The International Journal of Robotics Research*, vol. 28, no. 9, pp. 1118–1133, 2009.

[8] V. Egorov and A. P. Sarvazyan, "Mechanical imaging of the breast," *IEEE Transactions on Medical Imaging*, vol. 27, no. 9, pp. 1275–1287, Sep. 2008.

[9] B. Li, Y. Shi, A. Fontecchio, and Y. Visell, "Mechanical imaging of soft tissues with a highly compliant tactile sensing array," *IEEE Transactions on Biomedical Engineering*, vol. 65, no. 3, pp. 687–697, March 2018.

[10] X. Jia, R. Li, M. A. Srinivasan, and E. H. Adelson, "Lump detection with a gelsight sensor," in *2013 World Haptics Conference (WHC)*, April 2013, pp. 175–179.

[11] V. Jalkanen, B. M. Andersson, A. Bergh, B. Ljungberg, and O. A. Lindahl, "Prostate tissue stiffness as measured with a resonance sensor system: a study on silicone and human prostate tissue in vitro," *Medical and Biological Engineering and Computing*, vol. 44, no. 7, p. 593, 2006.

[12] C. Dagdeviren, Y. Shi, P. Joe, R. Ghaffari, G. Balooch, K. Usgaonkar, O. Gur, P. L. Tran, J. R. Crosby, M. Meyer *et al.*, "Conformal piezoelectric systems for clinical and experimental characterization of soft tissue biomechanics," *Nature materials*, vol. 14, no. 7, p. 728, 2015.

[13] H. S. Ryu, Y. H. Joo, S. O. Kim, K. C. Park, and S. W. Youn, "Influence of age and regional differences on skin elasticity as measured by the cutometer®," *Skin Research and Technology*, vol. 14, no. 3, pp. 354–358, 2008.

[14] H. P. Dobrev, "A study of human skin mechanical properties by means of cutometer," *Folia Med (Plovdiv)*, vol. 44, no. 3, pp. 5–10, 2002.

[15] B. Murray and R. Wickett, "Correlations between dermal torque meter®, cutometer®, and dermal phase meter® measurements of human skin," *Skin Research and Technology*, vol. 3, no. 2, pp. 101–106, 1997.

[16] K. Sangpradit, H. Liu, P. Dasgupta, K. Althoefer, and L. D. Seneviratne, "Finite-element modeling of soft tissue rolling indentation," *IEEE Transactions on Biomedical Engineering*, vol. 58, no. 12, pp. 3319–3327, 2011.

[17] H. Liu, D. P. Noonan, B. J. Challacombe, P. Dasgupta, L. D. Seneviratne, and K. Althoefer, "Rolling mechanical imaging for tissue abnormality localization during minimally invasive surgery," *IEEE Transactions on Biomedical Engineering*, vol. 57, no. 2, pp. 404–414, 2009.

[18] G. Boyer, L. Laquieze, A. Le Bot, S. Laquièze, and H. Zahouani, "Dynamic indentation on human skin in vivo: ageing effects," *Skin Research and Technology*, vol. 15, no. 1, pp. 55–67, 2009.

[19] G. Boyer, H. Zahouani, A. Le Bot, and L. Laquieze, "In vivo characterization of viscoelastic properties of human skin using dynamic micro-indentation," in *2007 29th Annual International Conference of the IEEE Engineering in Medicine and Biology Society*. IEEE, 2007, pp. 4584–4587.

[20] H. Zahouani, C. Pailler-Mattei, B. Sohm, R. Vargiolu, V. Cenizo, and R. Debret, "Characterization of the mechanical properties of a dermal equivalent compared with human skin in vivo by indentation and static friction tests," *Skin research and technology*, vol. 15, no. 1, pp. 68–76, 2009.

[21] K. A. Nichols and A. M. Okamura, "Autonomous robotic palpation: Machine learning techniques to identify hard inclusions in soft tissues," in *2013 IEEE International Conference on Robotics and Automation*, May 2013, pp. 4384–4389.

[22] H. Tran, F. Charleux, M. Rachik, A. Ehrlacher, and M. Ho Ba Tho, "In vivo characterization of the mechanical properties of human skin derived from mri and indentation techniques," *Computer methods in biomechanics and biomedical engineering*, vol. 10, no. 6, pp. 401–407, 2007.

[23] A. Dementyev, J. Hernandez, I. Choi, S. Follmer, and J. Paradiso, "Epidermal robots: Wearable sensors that climb on the skin," *Proc. ACM Interact. Mob. Wearable Ubiquitous Technol.*, vol. 2, no. 3, pp. 102:1–102:22, Sep. 2018. [Online]. Available: http://doi.acm.org/10.1145/3264912

[24] E. Sandford, Y. Chen, I. Hunter, G. Hillebrand, and L. Jones, "Capturing skin properties from dynamic mechanical analyses," *Skin Research and Technology*, vol. 19, no. 1, pp. e339–e348, 2013.

[25] C. T. McKee, J. A. Last, P. Russell, and C. J. Murphy, "Indentation versus tensile measurements of young's modulus for soft biological tissues," *Tissue Engineering Part B: Reviews*, vol. 17, no. 3, pp. 155–164, 2011.

[26] J. L. Sparks, N. A. Vavalle, K. E. Kasting, B. Long, M. L. Tanaka, P. A. Sanger, K. Schnell, and T. A. Conner-Kerr, "Use of silicone materials to simulate tissue biomechanics as related to deep tissue injury," *Advances in skin & wound care*, vol. 28, no. 2, pp. 59–68, 2015.

[27] Y.-L. Park, C. Majidi, R. Kramer, P. Bérard, and R. J. Wood, "Hyperelastic pressure sensing with a liquid-embedded elastomer," *Journal of micromechanics and microengineering*, vol. 20, no. 12, p. 125029, 2010.

[28] Formlabs. (2019) Materials data sheet. [Online]. Available: https://archive-media.formlabs.com/upload/XL-DataSheet.pdf

[29] E. Plastics. (2020) Delrin material properties. [Online]. Available: https://www.ejbplastics.com/pdf/ACETAL.pdf

[30] M. Abadi, P. Barham, J. Chen, Z. Chen, A. Davis, J. Dean, M. Devin, S. Ghemawat, G. Irving, M. Isard *et al.*, "Tensorflow: A system for large-scale machine learning," in *12th {USENIX} Symposium on Operating Systems Design and Implementation ({OSDI} 16)*, 2016, pp. 265–283.

[31] Z. Obermeyer and E. J. Emanuel, "Predicting the future—big data, machine learning, and clinical medicine," *The New England journal of medicine*, vol. 375, no. 13, p. 1216, 2016.

[32] Y. Taigman, M. Yang, M. Ranzato, and L. Wolf, "Deepface: Closing the gap to human-level performance in face verification," in *Proceedings of the IEEE Conference on Computer Vision and Pattern Recognition (CVPR)*, June 2014.

[33] A. Dementyev, "Dynamic wearable technology: designing and deploying small climbing robots for sensing and actuation on the human body," Ph.D. dissertation, Massachusetts Institute of Technology, 2019.

[34] A. Kalra, A. Lowe, and A. A. Jumaily, "An overview of factors affecting the skins youngs modulus," *Journal of Aging Science*, 2016.

[35] A. Kalra, A. Lowe, and A. Al-Jumaily, "Mechanical behaviour of skin: a review," *J. Mater. Sci. Eng*, vol. 5, no. 4, p. 1000254, 2016.

[36] Y. Zheng and A. F. Mak, "Effective elastic properties for lower limb soft tissues from manual indentation experiment," *IEEE Transactions on rehabilitation Engineering*, vol. 7, no. 3, pp. 257–267, 1999.

[37] A. F. Mak, G. H. Liu, and S. Lee, "Biomechanical assessment of below-knee residual limb tissue," *Journal of rehabilitation research and development*, 1994.

[38] A. Petron, J. Duval, and H. Herr, "Multi-indenter device for in vivo biomechanical tissue measurement," *IEEE Transactions on Neural Systems and Rehabilitation Engineering*, vol. 25, no. 5, pp. 426–435, 2017.

[39] B. J. Ranger, M. Feigin, X. Zhang, K. M. Moerman, H. Herr, and B. W. Anthony, "3d ultrasound imaging of residual limbs with camera-based motion compensation," *IEEE Transactions on Neural Systems and Rehabilitation Engineering*, vol. 27, no. 2, pp. 207–217, 2019.

[40] B. Lin, K. M. Moerman, C. G. McMahan, K. A. Pasch, and H. M. Herr, "Low-cost methodology for skin strain measurement of a flexed biological limb," *IEEE Transactions on Biomedical Engineering*, vol. 64, no. 12, pp. 2750–2759, 2017.

[41] K. M. Moerman, C. A. Holt, S. L. Evans, and C. K. Simms, "Digital image correlation and finite element modelling as a method to determine mechanical properties of human soft tissue in vivo," *Journal of biomechanics*, vol. 42, no. 8, pp. 1150–1153, 2009.